AAS 17-371

FROM SIMPLIFIED TO COMPLEX SMALL-BODY MODELS: SENSITIVITY ANALYSIS OF PERIODIC ORBIT SETS

Alex J. Pini[*], Benjamin F. Villac[†], and Rodney L. Anderson[‡]

A previous study introduced the use of clustering as a tool to support mission designers in organizing sets of ballistic orbits for small-body missions. In that study, periodic orbits generated in simplified dynamical models were examined, leading to the identification of attractive characterization orbits. This paper furthers that study by analyzing the sensitivity of these periodic orbits when exposed to various perturbations. In particular, the issue of transferring the initial conditions to higher fidelity models and the characterization of the resulting behavior is explored in light of the underlying dynamics. The asteroid 2008 EV5 is selected as a test case.

INTRODUCTION

The complexities associated with designing and operating a spacecraft mission in the vicinity of a primitive small body are well documented.[1] As the goals change from mission to mission, so do the trajectories utilized to accomplish the necessary tasks. While different classes of small-body orbits have been identified from past mission designs and astrodynamics research,[2–6] the exploration and organization of orbital options for a specific mission (and target small body) is still challenging. In particular, during the preliminary mission design or concept exploration phases, simplified dynamical models are often assumed to quickly enable a global overview of the available orbit types and geometry. Under these simplified models, periodic orbits are frequently used for a variety of purposes, such as the search for characterization orbit options via the use of clustering techniques,[7] which strive to organize large data sets into groups with similar attributes. In addition, periodic orbits found in simplified models can also serve as the foundation of orbital transfer design.[8,9]

The relatively large uncertainties in dynamical environments prior to first encounter on most asteroids, however, raise the question of the validity of using simplified models as approximations to the actual dynamics, and whether a preliminary transformation might help in improving the correspondence between simplified and realistic models. One justification for using simplified models is in the relatively small magnitude of the natural forces involved, enabling inexpensive active control in most orbital regimes to correct errors that arise from mis-modeling. For example, the concept of hovering over an asteroid surface has been studied[10–15] and somewhat demostrated in the case of the Hayabusa mission. The use of active control is not, however, always desirable, and orbits that provide long unperturbed observation times can also serve as attractive science orbits, such as with the terminator family and its variants.[5,16,17] The a priori determination of such "robust" behavior, or the estimate of the frequency of necessary active control, would thus be benefical in relating simplified solutions with concerns of the mission designer.

This investigation addresses the problem of periodic orbit sensitivity with respect to model parameters in small-body dynamical models. The approach is numerical and consists of a follow-on to the study by the authors on the clustering of periodic orbit databases.[7] In particular, this investigation assumes the availability of pre-computed sets of periodic orbits in simplified models (such as the Augmented Hill's 3-body Problem),

[*]Systems Engineer, a.i. solutions, Inc., NASA GSFC, B11 S222, Greenbelt, MD 20771
[†]Consulting Systems Engineer, a.i. solutions, Inc., 4500 Forbes Blvd. Suite 300, Lanham, MD 20706
[‡]Technologist, Jet Propulsion Laboratory, California Institute of Technology, 4800 Oak Grove Drive, M/S 301-121, Pasadena, CA 91109

and aims at characterizing the extent of the departure from the nominal periodic behavior when propagating these orbits in more realistic models, as periodic orbits cease to exist in such models. While the permissible level of departure from the nominal trajectory is dependent on the requirements of the particular mission, it is shown that classes of orbits which minimize the extent of the differences between simplified and more complex models can be extracted numerically.

This study focuses on smaller primitive bodies, using the asteroid 2008 EV5 as an example to illustrate the approach, as it was one of the destinations analyzed in the original study[7] and is currently the reference asteroid for NASA's Asteroid Redirect Mission.[18] A Generalized Elliptic Restricted 3-body Problem model with a rotating gravity field is used to emulate a realistic representation of the dynamics, as reviewed in the next section. The orbit sets considered are taken from the Augmented Hill's 3-body Problem with various acceleration magnitudes due to solar radiation pressure (SRP). As a first step, intrinsic orbital metrics that can be computed in the simplified model are considered. Then, multiple measures of an orbit's similarity to its nominal counterpart are defined and used globally on the orbit databases to characterize the sensitivity of the orbit set and the role played by each main perturbation (the eccentricity of the asteroid orbit, SRP strength, and non-uniform asteroid gravitational field). For each of these perturbations, the range of safe variations of the parameters is determined and mitigation strategies to transform the simplified orbits into similar orbits in the realistic model are considered. The study concludes with a summary of the findings and highlighted classes of robust ballistic orbits.

MODELING AND SAMPLE ORBIT SETS

Before discussing numerical simulations of periodic orbit behavior in the presence of perturbations, this section briefly presents the dynamical models used in this study, as well as the sample orbit data sets used in the sensitivity analysis presented in the follow-on sections.

Dynamical Models

In the precursor study to this investigation,[7] an Augmented Hill's 3-body Problem (AH3BP) was used to model the distant dynamics of a small body orbiter, while a rotating spherical harmonic model (SH) was selected for close proximity dynamics. These models can each be considered to be limiting cases of a Generalized Elliptic Restricted 3-body Problem (GER3BP), and the following paragraphs start by introducing this more general setting, which is used in the rest of the study. The simplified dynamical models utilized in the previous study are then briefly discussed in light of their relation to this more general model, notably with regard to scaling of the orbit initial conditions.

The Generalized Elliptic Restricted 3-Body Problem The GER3BP used in this study follows Refs. 19, 20 and provides a generic medium fidelity small-body orbiter dynamical model that includes the following time-varying effects: solar tides, SRP, the non-spherical gravity field of the small body, and the elliptical motion of the asteroid around the Sun.

Equations of Motion: The asteroid motion around the Sun is modeled as a Keplerian elliptical orbit and the Sun is represented as a point mass acting on the spacecraft. The equations of motion can be expressed in the rotating synodic asteroid orbit frame which is centered at the small-body center of mass. This frame, illustrated in **Figure 1**, has its x-axis pointing from the Sun to the asteroid, the z-axis along the asteroid's heliocentric orbital angular momentum vector, and the y-axis completing the direct, orthonormal frame.

Denoting the position vector of the orbiter as $\boldsymbol{r}$ (with the time derivative relative to the chosen rotating frame denoted by dots), the equations of motion can be written as:

$$\begin{aligned} \ddot{\boldsymbol{r}} = \quad & -2\boldsymbol{\omega}\times\dot{\boldsymbol{r}} - \boldsymbol{\omega}\times(\boldsymbol{\omega}\times\boldsymbol{r}) - \dot{\boldsymbol{\omega}}\times\boldsymbol{r} \quad + \ \boldsymbol{G}(\boldsymbol{r},t) \\ & + \tfrac{\mu_s}{|\boldsymbol{R}(f)|^3}\boldsymbol{R}(f) - \tfrac{\mu_s}{|\boldsymbol{R}(f)+\boldsymbol{r}|^3}(\boldsymbol{R}(f)+\boldsymbol{r}) \quad + \ \boldsymbol{A}_{SRP}(\boldsymbol{r},t) \end{aligned} \tag{1}$$

where $\boldsymbol{\omega}$ is the small-body orbital angular velocity and $\boldsymbol{R}(f)$ is its position relative to the Sun as a function of its true anomaly f. The term $\boldsymbol{G}(\boldsymbol{r},t)$ represents the rotating gravitational field of the asteroid and μ_s the

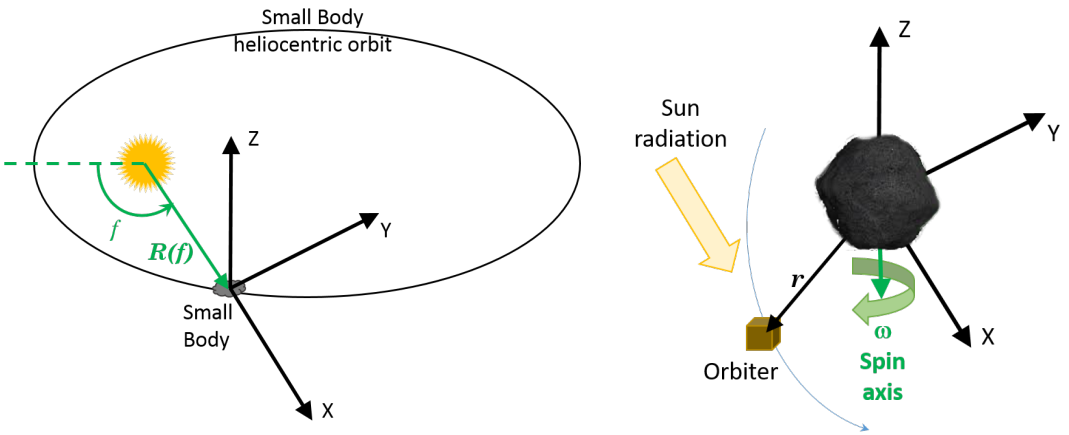

Figure 1. GER3BP frames. Left: Heliocentric view. Right: Small-body centered view.

gravitational parameter of the Sun. The vector $\boldsymbol{A}_{SRP}(\boldsymbol{r}, t)$ denotes the acceleration of SRP acting on the spacecraft.

In the case of 2008 EV5, the spin axis of the asteroid is nearly aligned with the negative of the orbital angular momentum vector and the approximation is made to align the body fixed z-axis with the $-z$-axis of the GER3BP. The gravitational acceleration, $\boldsymbol{G}$, is then obtained by expressing the force using spherical harmonics in the small-body-fixed frame and performing a coordinate transformation of the force computed using a rotation about the GER3BP $-z$-axis (with an angle varying linearly with time at the spin rate of the asteroid).

An 8^{th} degree and order gravity field has been used as a default field for 2008 EV5. The other orbital parameters used are given in **Table 1**. Because the location of the asteroid relative to other celestial bodies (aside from the Sun) is not considered in this research, the inclination, longitude of the ascending node, and argument of periapsis do not play a role in these equations. However, the non-zero eccentricity does play a role in modulating the Sun's influence (both as SRP and as gravitational acceleration) on the orbiter.

Parameter	Value	Parameter	Value
Eccentricity	0.084	μ ($\frac{km^3}{s^2}$)	4.69e-9
Perihelion Dist. (AU)	0.878	Asteroid Radius (m)	202.607
Inclination (deg)	7.437	Rotation Period (h)	3.725
Long. of Asc. Node (deg)	93.399	Pole Long. (deg)	180
Arg. of Perihelion (deg)	234.803	Pole Lat. (deg)	-84 $\pm$10

Table 1. Dynamical and physical parameters for 2008 EV5 (from Ref. 21).

The SRP acceleration is modeled here as a flat plate always facing the Sun and can be expressed as:

$$\boldsymbol{A}_{SRP}(\boldsymbol{r}, t) = \frac{\mu_{SRP}}{|\boldsymbol{R}(f) + \boldsymbol{r}|^3}(\boldsymbol{R}(f) + \boldsymbol{r}) \quad \text{with} \quad \mu_{SRP} = G_{SRP}\frac{A}{m}(1 + \rho) \tag{2}$$

The value of G_{SRP} is taken as 10^8 $km^3kg/(s^2m^2)$. The term A/m is the area-to-mass ratio, which is also considered in the calculation of the normalized SRP acceleration β in the AH3BP, and ρ is reflectance of the plate (taken to be 0.01 $\frac{m^2}{kg}$ and 0.15, respectively for a baseline β of 27). In essence, the acceleration due to SRP has an equivalent effect of reducing the Sun's gravitational acceleration on the spacecraft via a reduction in the Sun's mass. However, the asteroid's orbit is considered to be unaffected in this model, as it proceeds according to Keplerian motion.

Limitations and Key Features: While the above model does add some realism to the dynamics of a small-body orbiter (compared to the simplified models used in the previous study), the formulation is still only approximate, with notable simplifications in the SRP effect. In particular, shadows cast by the small body are not accounted for, nor are the expected fluctuations due to the spacecraft attitude changes occurring in an actual mission. However, these simplifications are representative of the inherent uncertainty in small-body orbiter dynamics. Beyond the typical unknown variation of the SRP accelerations due to attitude changes at this design stage, other parameters such as the small-body gravity field and pole orientation may also not be known to the precision considered here when launching the mission. The use of a particular set of parameters should thus only be interpreted as a sample in a set of potential models, and the above model represents a middle-ground between quite simplified models and high fidelity scenarios.

The GER3BP model notably adds significant complexity compared to the AH3BP or uniformly rotating gravitational field used in the previous study, and the coupling of the forces mentioned above results in a time-varying model with no integral of motion. Consequently, periodic orbits cease to exist, even though quasi-periodic orbits with similar characteristics are possible. This time variation also prevents the existence of equilibria, though libration point regions can still be found. Another effect of the time-varying character of these dynamics is the addition of an extra parameter in the study of the problem: the same AH3BP initial conditions will generally evolve in different ways when the small body is at perihelion and aphelion. The time of perihelion passage of the asteroid must then be taken into consideration when applying the initial conditions saved in the orbit database. This phenomenon is explored further in the following section.

Close proximity dynamics approximation When approaching the small body, the relative magnitude of the term $\boldsymbol{G}(\boldsymbol{r}, t)$ increases and can dominate all the other forces. While the region at which this term dominates is dependent on the asteroid and the spacecraft, it has been estimated to be within a few asteroid radii in the case of 2008 EV5.[7] In that region of space, the SRP and Sun influence can be ignored, leaving the dynamics approximated by a rotating, non-uniform gravitational field. The motion of the asteroid around the Sun can be ignored for time scales that are small compared to the orbital period of the asteroid. Since the rotational period for EV5 is on the order of a few hours (compared to an orbital period of roughly a year), there is a range of time and space where the rotating gravity field can be applied. In Ref. 7, these dynamics were thus expressed in the asteroid body frame, and the resulting system becomes Hamiltonian and time-invariant:

$$\mathcal{H} = \frac{1}{2}((p_x + \omega_{pole} y)^2 + (p_y - \omega_{pole} x)^2 + p_z^2) - \frac{1}{2}\omega_{pole}^2 (x^2 + y^2) - U(x, y, z) \tag{3}$$

where U represents the gravitational potential and ω_{pole} is the scalar rotation rate of the asteroid around its pole. Equilibria with associated periodic orbit families can then be computed, as illustrated in **Figure 2**.

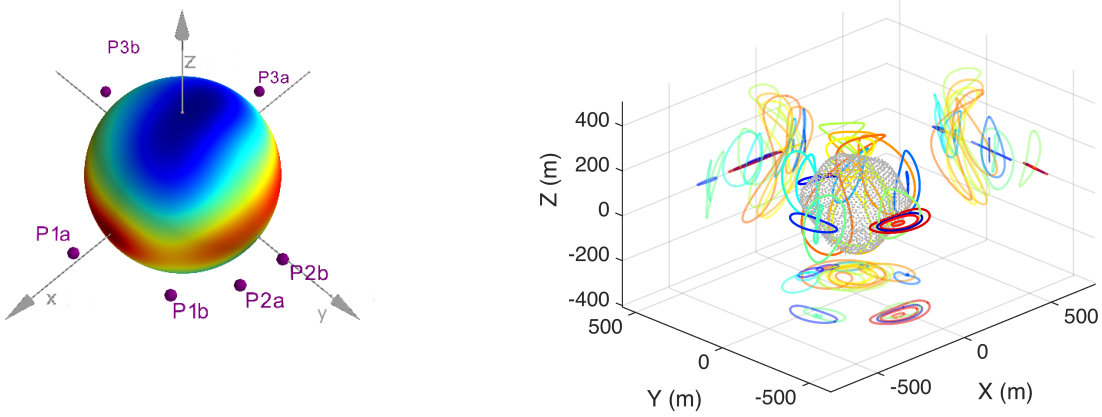

Figure 2. Left: Representation of EV5 gravitational potential with relative equilibria. Right: Sample orbits for a rotating non-spherical gravity field. The axes are the body fixed axes associated with the spherical harmonic models used.

When considering the dynamics in the GER3BP frame, however, these periodic orbits appear, at best, as quasi-periodic since a new frame frequency is introduced (even when the other perturbing forces are not accounted for). The transformation of position coordinates between the body-fixed and GER3BP frame in particular involves a rotation about the z-axis with a flip of the axis given the approximation on the spin axis of EV5 relative to the orbital angular momentum. More precisely, by denoting $\Theta_p(t)$ the longitude of the small-body pole axis in the GER3BP frame, λ_p its latitude (time invariant), and $\theta(t)$ the longitude of the body fixed x-axis relative to an appropriate equatorial inertial frame, the spacecraft position coordinates in the GER3BP frame, R_c, and those in the body fixed frame, r_c can be expressed as:

$$R_C = \mathcal{R}(t) r_c = \mathcal{R}_z(\Theta_p(t)) \mathcal{R}_y(\lambda_p - 90^\circ) \mathcal{R}_z(-\theta(t)) r_c \tag{4}$$

where $\mathcal{R}_y(.)$ and $\mathcal{R}_z(.)$ represent the rotation matrices about the second and third axis, respectively. For EV5, approximating the pole latitude λ_p to be -90^o, this relation simplifies to:

$$R_C = \mathcal{R}(t) r_c = \mathcal{R}_y(180^\circ) \mathcal{R}_z(-\Theta_p(t) - \theta(t)) r_c \tag{5}$$

Note that the angle $\psi(t) = -\theta(t) - \Theta_p(t)$ can be obtained by integrating the equation:

$$\frac{d\psi}{dt} = -\omega_{pole} - \frac{df}{dt} \quad \text{with} \quad \frac{df}{dt} = \frac{h}{r^2} = \sqrt{\frac{\mu}{p^3}} \left(1 + e\cos f\right)^2 \tag{6}$$

In practice, for short periods of time, the term $\frac{df}{dt}$ can be taken as a constant (set at the initial condition epoch t_0), so that $\psi(t)$ can be approximated by:

$$\psi(t) = \left(-\omega_{pole} - \frac{df}{dt}\right)(t - t_0) \tag{7}$$

Regarding the velocity transformation, denoting $\dot{\boldsymbol{r}}$ as the spacecraft velocity vector in the GER3BP and $\boldsymbol{r}'$ as the velocity vector in the body fixed frame, $\dot{\boldsymbol{r}} = \boldsymbol{r}' + \boldsymbol{\omega_{rel}} \times \boldsymbol{r}$, where $\boldsymbol{\omega_{rel}} = \boldsymbol{\omega_{pole}} - \boldsymbol{\omega}$ is the angular velocity of the body fixed frame relative to the GER3BP frame. In the approximation $\lambda = -90^\circ$, this angular velocity is aligned with the $-z$-axis of the GER3BP frame, so that $\omega = -\omega_{pole} - \frac{df}{dt}$. When expressing these relations in coordinates, the rotation matrix $\mathcal{R}(t)$ should be used to transform coordinates between the body fixed and GER3BP frames.

Distant dynamics approximation When in a distant neighborhood of the asteroid (past tens of asteroid radii), the non-uniform gravity field can be approximated by a point mass and the gravitational attraction of the Sun on the spacecraft can be linearized. When the asteroid eccentricity is set to zero, the Augmented Hill's 3-body Problem (AH3BP) that has been used in the previous study[7] is recovered. In that case, the SRP acceleration is expressed as $\beta\hat{\boldsymbol{x}}$ where $\hat{\boldsymbol{x}}$ is the unit vector along the x-axis of the synodic frame and β measures the level of SRP affecting the spacecraft. This definition leads to an autonomous Hamiltonian system where a multitude of periodic orbits can be computed and used in exploring mission concepts. Scaling the time and length units as $T = \left(\frac{a^3}{\mu_s}\right)^{1/2}$ and $L = a\left(\frac{\mu}{\mu_s}\right)^{1/3}$, respectively, (where a represents the semi-major axis of the asteroid orbit) leads to a normalized problem with β as the only parameter. The Hamiltonian of the system can then be written as:

$$\mathcal{H} = \frac{1}{2}\left((p_x + y)^2 + (p_y - x)^2 + p_z^2\right) - \Omega \quad \text{where} \quad \Omega = \frac{1}{2}\left(3x^2 - z^2\right) - \frac{1}{r} - \beta x \tag{8}$$

and where p_x, p_y, p_z represents the coordinates of the momenta in the synodic frame. In the sample scenario considered in Ref. 7, a normalized β value of 27 was used to represent the relative magnitude of the SRP with the point mass gravity of EV5, and this case will continue to be considered in the following sections. **Figure 3** presents a few of the orbit families computed in this problem using both continuation methods and grid search techniques.

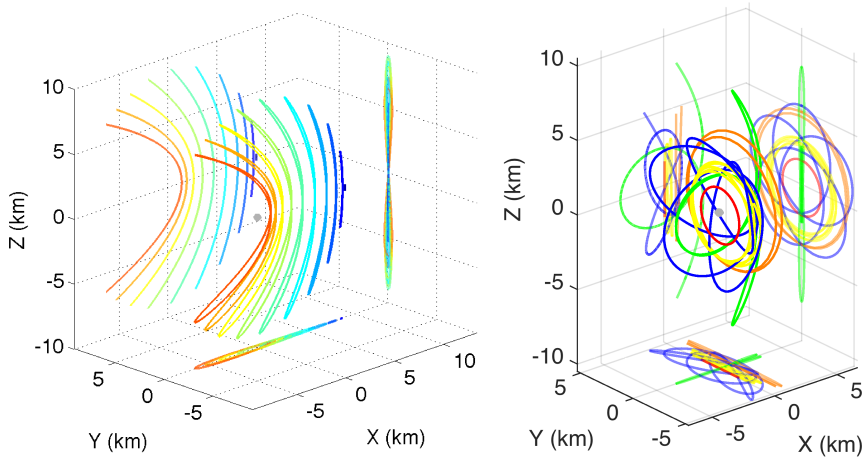

Figure 3. Sample periodic orbits in the (circular) AH3BP for $\beta = 27$ (from Ref. 7). Left: Vertical family associated with L2. Right: Sample orbits from a grid search.

In contrast to the circular problem, when the eccentricity is considered, the system is no longer time-invariant and the SRP strength becomes a function of the asteroid position in its orbit. In particular, an approximate expression of the AH3BP equivalent SRP ($\beta(f)$) for a given asteroid position on its orbit is obtained by solving $\frac{\mu_{SRP}}{R^2(f)} = \beta(f)\frac{L(f)}{T(f)^2}$, where $L(f)$ and $T(f)$ correspond to the now time-varying equivalent length and time units. The solution can be expressed as:

$$\beta(f) = \frac{\mu_{SRP}}{\mu^{1/3}\mu_s^{2/3}}\left(\frac{a}{R(f)}\right)^2 = \beta_0\left(\frac{1+e\cos(f)}{1-e^2}\right)^2 \tag{9}$$

where β_0 represents the SRP in the circular AH3BP having the same semi-major axis as the elliptic problem. While this correspondence is only approximate (since it ignores the motion of the spacecraft), it does capture the time variation of SRP in the GER3BP and shows that a constant SRP area in the GER3BP is equivalent to a time varying SRP area in an AH3BP model (and vice versa). An important takeaway from **Equation 9** is that for a given value of β_0, the variation of $\beta(f)$ is only a function of the eccentricity of the orbit and not the semi-major axis. **Figure 4** notably presents the relative difference between the β at perihelion and aphelion and β_0 (expressed as percentages).

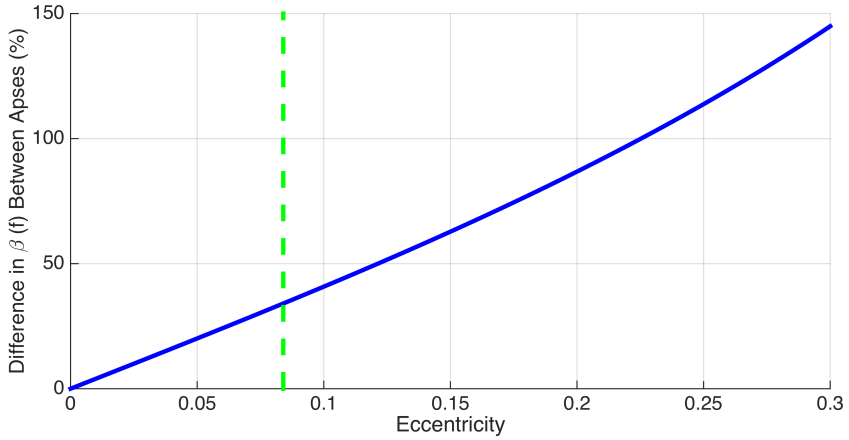

Figure 4. Normalized SRP coefficient difference between peri- and aphelion as a function of the asteroid eccentricity (nominal AH3BP value: $\beta = 27$). The dashed green line represents the eccentricity of EV5's orbit.

This variation can be shown to change according to $\frac{2e}{(1-e^2)^2}$ and thus increases quite fast. For an eccentricity of 0.25, the difference in SRP between the apses is larger than the nominal value on a circular orbit. In the case of EV5, where the orbit eccentricity is about 0.084, for a circular β_0 value of 27, the periapsis β value is ~ 32 and the aphelion value is ~ 23. This variation represents a difference of 34% compared to the selected representative nominal value of 27. This difference is already quite large, and we can expect that the variation in SRP with the asteroid location will significantly affect the behavior of the periodic orbits found in the circular case.

Even without SRP present, the direct application of initial conditions from a circular Hill's problem to an elliptic problem would be affected by the eccentricity of the orbit. However, this effect can be mitigated by using pulsating coordinates that normalize the elliptic problem. More precisely, selecting the length scale of the problem to be:

$$L = \left(\frac{\mu}{\mu_s}\right)^{1/3} \frac{a(1-e^2)}{1+e\cos f} \tag{10}$$

and the independent time variable to be the asteroid true anomaly (so that time and normalized time are related by $df = \sqrt{\frac{\mu_s}{p^3}}(1+e\cos f)^2 dt$), leads to the same location of the libration points in the circular and elliptic case when no SRP is present. A notable caveat to this relationship is that the position of these libration points are moving (or pulsating) in physical coordinates according to the true anomaly of the asteroid in its heliocentric orbit. As will be seen in a later section, scaling the periodic orbit initial conditions computed in the AH3BP in this fashion often leads to more similar behavior in the GER3BP.

Periodic Orbit Data Sets

In order to evaluate the sensitivity of periodic orbit sets to changes in model parameters, one of the periodic orbit databases used in Ref. 7 has been revisited. This database consists of periodic orbits calculated in the AH3BP model using grid search techniques, although another database constructed via continuation and bifurcation was available. While the continuation and bifurcation approach resulted in a less exhaustive set of orbits than the grid search technique, it provided solutions in the rotating spherical harmonic model where the grid search could not succeed. In the following, focus has been given to the AH3BP orbit set as obtained by grid search.

Raw orbit data sets:

The initial orbit database (consisting of 2552 sets of periodic orbit initial conditions) was first pruned to remove orbits with obvious unsatisfactory characteristics for the sample problem considered. For example, periodic orbits that were too large to provide reasonable observation of an asteroid or cross below the surface of EV5 were identified and removed. The resulting pruned set contains 2081 candidate orbits that need to be further trimmed based on both misson objectives and robustness to uncertain model parameters. Some orbits considered were already presented in **Figure 2** and **Figure 3**, but they are more generically represented by associating a single point to each orbit. **Figure 5 (left)**, for example, shows each orbit by its closest periapsis location in the AH3BP frame. **Figure 5 (right)** presents the orbits by their values of closest periapsis radius and furthest apoapsis radius, and colored by orbital period values.

The orbit set can be clearly seen to be organized into periodic orbit families of similar periods and apses characteristics. In particular, a short period family with very low periapse radii (dark blue, with nearly 0 minimum periapsis in **Figure 5 (right)**) corresponds to highly eccentric orbits, while the family appearing as a nearly straight diagonal line corresponds to the well-known terminator family. In addition to this set, periodic orbits in the Hill's 3-body Problem (H3BP, where $\beta = 0$) have also been considered to facilitate the analysis of the relative scale of the various perturbations in the upcoming sections. This orbit set is presented in **Figure 6**. Surprisingly, the orbit set computed in the H3BP (using the same search and correction approach as in the AH3BP) led to fewer orbits, clearly concentrating on a few orbit families corresponding mostly to planar near-circular families and large halo orbits.

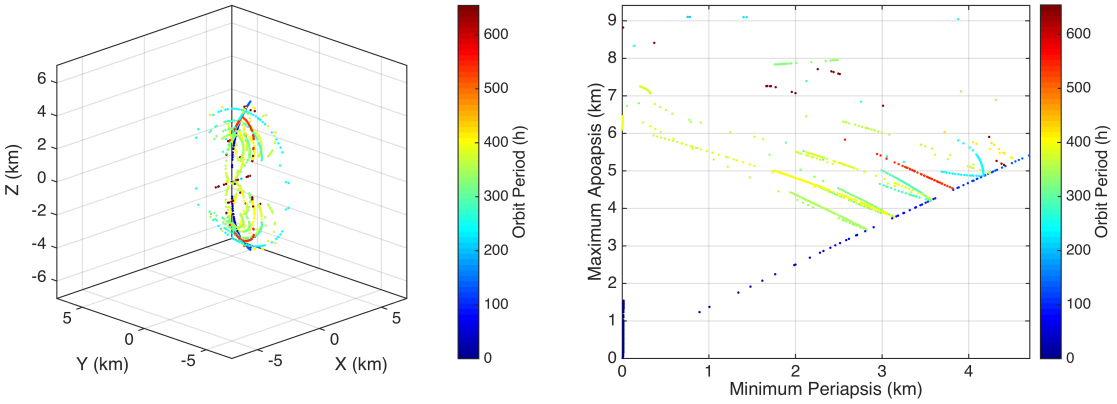

Figure 5. Representation of the initial orbit set by their closest periapsis. Left: Periapsis position in the AH3BP frame. Right: Projection in periapsis-apoapsis space.

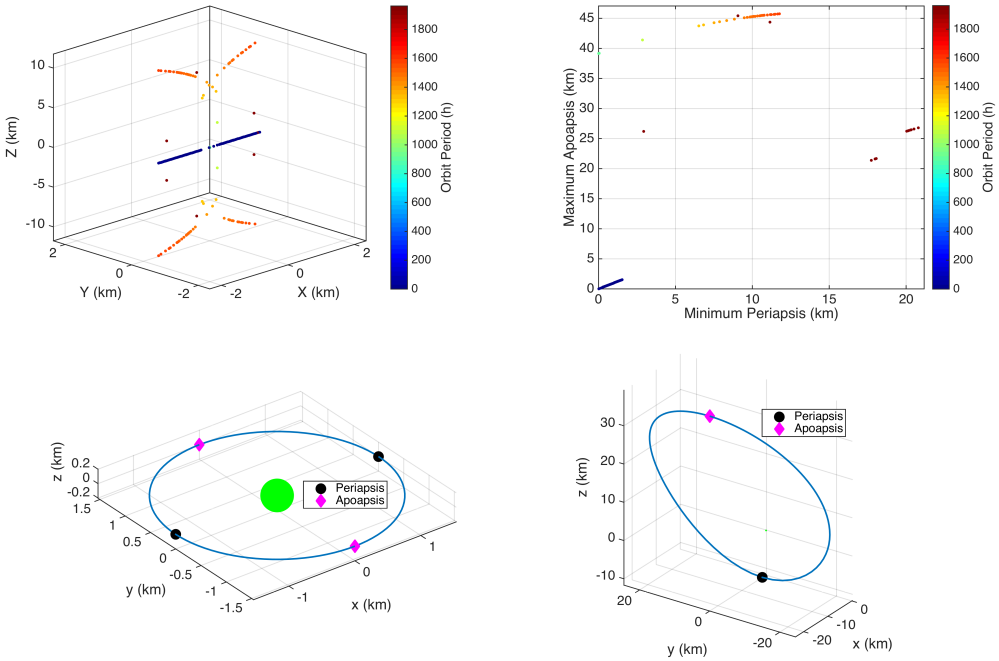

Figure 6. Overview of the H3BP orbit set. Top Left: Closest periapsis representation of the H3BP periodic orbit set considered. Top Right: Periapsis-apoapsis representation. Bottom Left: Sample close-periapsis planar orbit. Bottom Right: Sample large periapsis halo orbit.

Intrinsic metrics: During the grid search process used to construct the raw databases, when a periodic orbit is found, the initial conditions are logged along with the orbital period, Jacobi constant, and maximum eigenvalue of the monodromy matrix.[7] In addition, the databases are post-processed and augmented by computing intrinsic metrics to help predict the sensitivity with respect to model parameters. For the AH3BP, the only model parameter is the normalized SRP coefficient β, and only the partial with respect to that parameter has been considered in this simplified model. That is, if $\dot{X} = F(X, \beta)$ represents the state dynamics in the AH3BP, the sensitivity with respect to β is computed by propagating **Equation 11** and saving the maximum

2-norm of that sensitivity vector ($||\partial X/\partial\beta||$), referred to as the "sensitivity index", over the integration time span:

$$\frac{d}{dt}\frac{\partial X}{\partial \beta} = \frac{\partial F}{\partial X}(X(t),\beta) + \frac{\partial F}{\partial \beta}(X(t),\beta) \tag{11}$$

where $\frac{\partial X}{\partial \beta} = 0$ at the initial epoch. While the AH3BP can be thought of as a simplified case of the GER3BP (for $e = 0$ and a point mass gravity field) and partial derivatives of the other GER3BP model parameters could be assessed, the approach taken in this study is more numerical and considered other metrics that can be computed solely from the nominal AH3BP orbits (described below). In particular, the use of the parameter derivatives alone only predicts perturbations over very small ranges of values, and a combination of factors has been considered to characterize the overall orbit set changes.

In addition to more "standard" intrinsic metrics (such as minimum periapsis, maximum apoapsis, and maximum Lyapunov exponent throughout the course of the orbit), other metrics that are analogous to Keplerian elements are computed. For instance, a proxy for the periodic orbit's eccentricity (referred to as the "surrogate eccentricity") is calculated via the classical two-body relationship, except the minimum periapsis and maximum apoapsis of the periodic orbit are used in place of their lone counterparts. To form a representation of the orbital angular momentum, the length and area swept out by the spacecraft's position vector throughout the course of the trajectory have also been considered. The area, $\mathcal{A}$, is notably used to derive the "surrogate angular momentum", $h_{sur} = 2\frac{\mathcal{A}}{T}$, where T represents the orbital period. With these preliminaries completed, the next step consists of investigating the effect of perturbations when the orbits are propagated in the GER3BP.

SINGLE ORBIT SENSITIVITY CHARACTERIZATION

The periodic orbit sets presented in the previous section assumed simplified dynamics, and the propagation of these initial conditions in the GER3BP does not lead to closed orbits. The extent of the effect of these perturbations on the orbits depends on several factors, including the way these effects are measured. This section considers sample periodic orbits to highlight these issues and describe the measures selected for quantifying these effects.

Single orbit behavior

The periodic orbits that were found in the AH3BP cannot remain periodic in a medium fidelity model that accounts for several additional perturbations, such as those captured in the GER3BP. However, as shown in **Figure 7**, orbits may exhibit varying degrees of divergence from their "nominal" trajectories that depend on the orbital geometry and asteroid's distance from the Sun, among other factors.

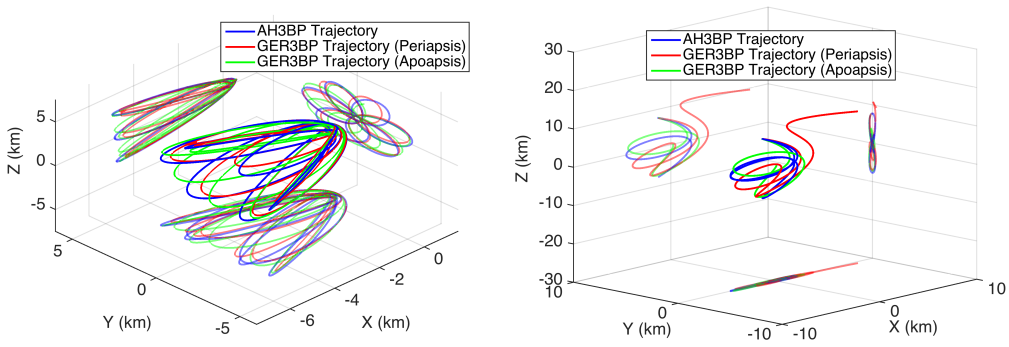

Figure 7. Individual cases representing the spectrum of orbit behavior whenever the AH3BP periodic initial conditions ($\beta = 27$) are propagated in the GER3BP. For some orbits, the general shape is maintained regardless of the asteroid location (left), but others tend to be more sensitive to the dynamics (right).

For instance, **Figure 7 (left)** shows a Sun-side resonant terminator orbit that appears to retain its shape when propagated for one orbital period ($\sim$31 days) in the GER3BP, regardless of the level of SRP acceleration that arises from the asteroid's heliocentric orbital location. Alternatively, some orbits rely on a delicate balance of SRP and gravitational accelerations to maintain periodicity. This sensitivity can be seen in **Figure 7 (right)**, where the AH3BP periodic vertical orbit starts to lose its shape after one period ($\sim$27 days) and eventually collides with the asteroid when the asteroid is at aphelion and the SRP acceleration decreases. At perihelion, the increased SRP acceleration causes the spacecraft to diverge away from the asteroid relatively quickly.

Similar results apply to the H3BP case ($\beta = 0$) when transferring the initial conditions to the GER3BP with no SRP, as the introduction of the asteroid orbit's eccentricity alone is often sufficient to result in diverging behavior. From a preliminary mission design standpoint, a practical goal is to establish a way to predict the likelihood of divergence in the perturbed model from the value of intrisic orbit metrics as computed in the simplified model (such as the ratio between apoapsis and periapsis, maximum Lyapunov exponent, orbit "area", and Jacobi constant). A better understanding of the role played by the asteroid parameters (such as eccentricity and location on its orbit) in the diverging cases would also help in better using the simplified dynamics in mission design. For the perturbation levels considered here, the transformation of orbit initial conditions from the AH3BP coordinates to the GER3BP, as well as the potential variation of initial conditions on a given nominal orbit, both play a role. However, taking the initial state at either periapsis or apoapsis seems to bound the range of motion dependent on the initial "phase" of the periodic orbit and the following analysis will therefore focus only on the state transformations and dependence on the asteroid model parameters.

Quantifying orbit behavior

To help identify the driving forces behind a particular orbit's sensitivity to model parameter discrepancies, a method of quantifying a perturbed orbit's similarity to its AH3BP counterpart will first be established. There are many different ways to define the similarity between two curves, but those described in this study operate on the difference in position vectors between the two orbits, which will be referred to as position errors from the nominal periodic AH3BP trajectory. To properly compare the orbits, the results of their propagations are reported at commensurate time steps, and the position vectors are converted to equivalent units (kilometers in this case). The magnitude of these position errors computed at each integration time, t_i, as expressed in **Equation 12**, forms the foundation of the error metrics used in this study:

$$d_{err}(t_i) = \|\boldsymbol{r}_{pert}(t_i) - \boldsymbol{r}_{nom}(t_i)\| \tag{12}$$

where $\boldsymbol{r}_{pert}(t_i) - \boldsymbol{r}_{nom}(t_i)$ is the position error vector between the perturbed and nominal periodic trajectories, respectively, and $d_{err}(t_i)$ is the size of this error at time t_i. It should be noted that although only the position-based errors are utilized in this study, developing metrics based on other information (such as the velocity) could potentially provide more insight into the extent in which orbits depart from their nominal trajectories. Also, the metrics selected considers errors as measured at particular times, rather than distance between orbits. As a results, larger errors values due to the typical drift along track of nearby orbits is expected than would be for distances measured between orbits.

The nominal periodic orbits that are considered for this investigation vary considerably in size, shape, and period. Because of this variation, using only the raw position errors (or their magnitudes) to compare the sensitivities of two arbitrary orbits may be misleading. Examining the sensitivity of a perturbed orbit after one period is a natural choice for the propagation length because a better picture of the full dynamical behavior can be observed. If two arbitrary orbits with vastly different sizes and periods are compared, the raw position errors will tend to be smaller after one period for the smaller orbits (which tend to have shorter periods), as the errors will not have as much time to accumulate. To enable better comparison across the spectrum of orbits, the error calculation should be normalized such that it is less dependent on the orbit size and propagation time.

For instance, scaling $d_{err}(t_i)$ by the nominal orbit's range at the point of evaluation effectively yields a measure of the position error in terms of orbital "radius," which is better suited for comparison across a set of

orbits with a wide variety of sizes. This relative error may fluctuate in different ways over one period, so the highest ratio that is observed throughout the course of the trajectory is considered, resulting in the following error metric:

$$\eta = max\left(\frac{d_{err}(t_i)}{\|\boldsymbol{r}_{nom}(t_i)\|}\right) \tag{13}$$

The term η in **Equation 13** helps to evaluate the sensitivities of large and small orbits in a similar fashion and will be referred to as the max error ratio between the two orbits. To account for the variations in orbital period (and therefore propagation time for the errors to grow), a metric which normalizes over time can also be devised. First, the area under the curve (α) created by $d_{err}(t_i)$ as a function of time can be computed via the trapezoidal rule to obtain the total integrated error, which is independent of the propagation print interval. This integrated error can then be divided by the nominal orbital period to arrive at the average integrated error over the orbit (γ):

$$\gamma = \frac{\alpha}{T} \tag{14}$$

where T is the total period of the orbit in seconds. The max error ratio η and average integrated error γ form two separate error metrics that help to eliminate systematic inaccuracies that may arise from the orbit size and period, respectively, and allow the sensitivity of the orbits to be compared in terms of their underlying dynamical properties. As such, these metrics are used as a method of quantifying the behavior of the orbit set in the presence of perturbations. For instance, they can be used to categorize orbits as staying bounded or diverging for pruning purposes by assigning a threshold for the levels of permissible relative errors. They are also helpful in identifying the driving perturbation sources for different types of orbits, as shown in the next section.

Perturbation relative scales

The GER3BP models a variety of perturbations, all of which could cause the periodic orbits that were found assuming AH3BP dynamics to depart from their nominal trajectories. The magnitudes of these perturbing accelerations depend on the regime of motion of the orbit in question, so the primary perturbation source will vary according to the orbit's properties (such as size and location). The error metrics established in the previous section can be used to compare the effects of these perturbations by observing the errors that are induced under individual perturbation sources.

To quantify the sensitivity to each perturbation, the GER3BP model is configured to replicate the AH3BP dynamics under which the periodic orbit was originally found by setting the asteroid gravity to a point mass, circularizing the asteroid orbit, and matching the SRP acceleration that was modeled in the AH3BP. Then, the different perturbation sources are enabled one at a time with increasing magnitude, the orbit is propagated for one period, and the error metrics are calculated for each case to characterize the sensitivity of a particular orbit to the individual perturbation. To illustrate how each perturbation can vary in significance for different trajectories, two dissimilar orbits were selected as test cases, as shown in **Figure 8**.

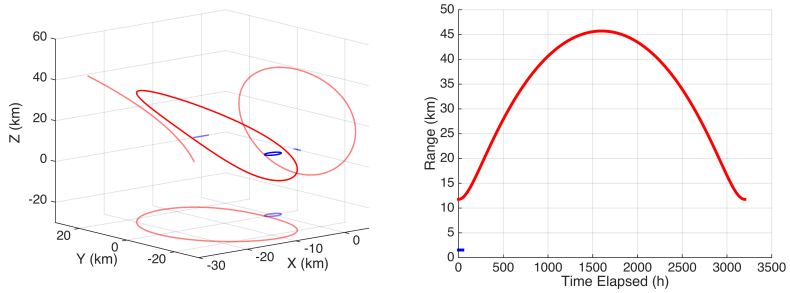

Figure 8. Left: Two unique orbits that were used as test cases to identify the relative size of individual perturbation sources. Right: The range of each periodic orbit throughout one period.

The two orbits in **Figure 8** were obtained from the H3BP data set ($\beta = 0$) and selected due to their difference in size, shape, period, and orbital regime. The blue orbit is a relatively small, nearly circular planar orbit with a radius of ∼1.5 km and a period of ∼48 hours. The red orbit is much larger with a range varying between 12 and 46 km, has a longer period (∼133 days), and exhibits an out of plane component. These orbits also differ in that the red orbit resides solely on the sun-lit side of the asteroid (the X-component in AH3BP frame is always negative), while the blue orbit spends an equal amount of time in sunlight and darkness.

For this analysis, four different perturbation sources were tested individually: solar radiation pressure, the fidelity of the asteroid's spherical harmonic gravity model, asteroid orbit eccentricity, and the true anomaly of the asteroid in its orbit. For an arbitrary perturbation source, by starting with zero perturbation magnitude and gradually increasing the effect, the evolution of the orbit's sensitivity to that type of perturbation can be observed. The non-spherical gravity perturbation requires slightly different treatment, as the fidelity of the asteroid's spherical harmonic gravity model is being increased. That is, the degree and order of the model are considered always equivalent and increased from 1×1 to 8×8. Also, since true anomaly is undefined for a circular asteroid orbit (which is assumed by the AH3BP), a small eccentricity must be applied to the asteroid orbit before varying the true anomaly. The maximum perturbation sizes for eccentricity and SRP (normalized β) were selected to be 0.1 and 10, respectively, as these are roughly what can be expected for the case of EV5. By repeating this incremental process for each of the sources and comparing the behavior of the resulting error metrics as the perturbations grow larger, the driving perturbations for that orbit can be identified, as shown in **Figure 9**.

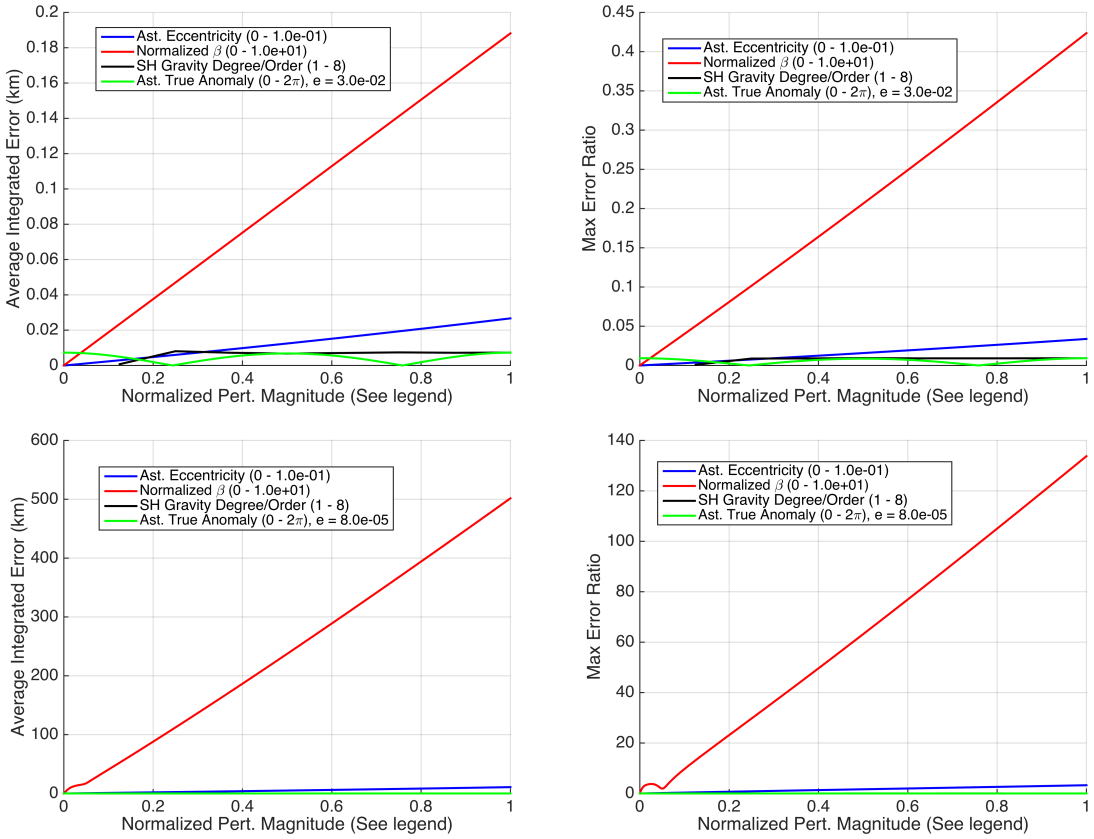

Figure 9. Evolution of the induced errors to each of the major perturbations for the two test orbits shown in Figure 8. The abscissa (perturbation size) is normalized by the maximum value to enable comparison between the multiple sources. The top row corresponds to the small blue planar orbit and the bottom row is the larger red orbit. Note the difference in the y-axis scale between the various plots.

The left and right columns of plots in **Figure 9** correspond to the two error metrics (average integrated error and max error ratio, respectively) that were introduced in the previous section. The most notable conclusion that can be drawn from **Figure 9** is that the driving perturbation for both orbits in terms of sensitivity is by far the SRP acceleration (red line), as a variation in normalized β of 10 resulted in errors at least an order of magnitude worse than the maximum perturbations from the other sources. Also, the asteroid orbit's eccentricity (blue) is more influential than the fidelity of the gravity model (black) for the range of perturbation magnitudes that were tested.

The error information presented in **Figure 9** provides a good overview of the dominant perturbations and their relative importance to the two types of orbits. However, the scales of the errors can be difficult to infer from these plots alone, particularly for the bottom row, which corresponds to the large red orbit. Another way to contextualize this error information is to determine the perturbation size bounds for each source that will result in similar error magnitudes. As seen in **Figure 10**, the upper bound of the eccentricity and SRP perturbations generally needs to be reduced to the point where the errors can match those of the non-spherical gravity, which appears to be fairly independent of the higher order degree and order terms.

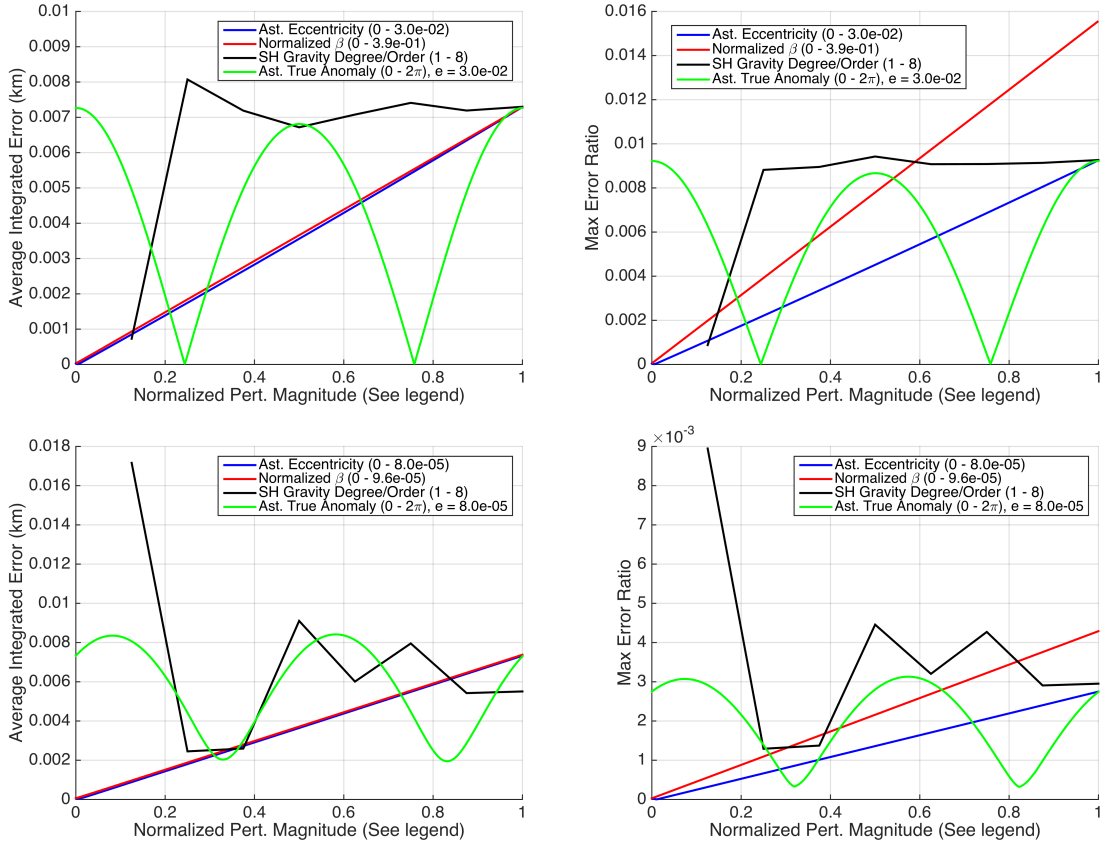

Figure 10. Evolution of the induced errors for relatively small perturbations. The upper bounds of the perturbation sizes are individually selected for each source such that the resulting error magnitudes are roughly equivalent. The top row corresponds to the small blue planar orbit, and the bottom row is the larger red orbit.

The range of perturbations in which the error magnitudes are similar is relatively small (a maximum eccentricity of 0.03 and normalized β of 0.39 among both orbits), regardless of the shape/size of the nominal orbit. Due to the size of the large red orbit, the non-spherical gravitational force will intuitively have less of an influence on the motion of the spacecraft, as the gravity field more closely resembles a point mass than at closer

ranges. As a result, the sensitivity to a modeling difference in these spherical harmonic parameters is much smaller for the large orbit than it is for the smaller blue orbit that remains in close proximity to the asteroid. The bottom left plot in **Figure 10** illustrates that the large test orbit is far more sensitive to perturbations in eccentricity and SRP than it is to mis-modeling of the gravity field, as evidenced by the very low bounds on eccentricity and normalized β that are needed to produce similar error levels. For the smaller blue orbit (top row), there appears to be a more "balanced" sensitivity between the non-spherical gravity, eccentricity, and SRP perturbations than there is for the large halo orbit.

In addition to providing some insight about how well AH3BP periodic orbits will translate to a high-fidelity model accounting for these perturbations, these results can also be interpreted in terms of the permissible level of fidelity necessary for an accurate representation of the dynamics in these types of environments. For instance, the high sensitivity to changes in SRP acceleration emphasizes the importance of correctly modeling this perturbation and suggests that a higher fidelity spacecraft attitude-dependent box and wing model will yield important information regarding the perturbed orbit behavior. However, in the case of larger orbits, the effects of using a gravity model beyond 8×8 may not be as profound.

These two test orbits offer some insight into general trends regarding the importance of the various major perturbations, but do not represent the entirety of the different orbit shapes and sizes contained in the data set. These principles will be used in the following section in order to gather large-scale information about the sensitivity of the whole set in an attempt to find patterns.

SENSITIVITY OF ORBIT SETS AND MITIGATION STEPS

With the orbital sensitivity measures defined, this section investigates the global behavior of periodic orbit data sets. In particular, global measures defined on the data sets are discussed and used to characterize the relative effect of each perturbation overall. Mitigation strategies to limit the destruction of the original periodic orbit set are then discussed in relation to individual perturbation sources.

Orbit set sensitivity measures and behavior clusters

As discussed in the previous sections, a single orbit's behavior can be characterized by metrics intrinsic to the simplified model (AH3BP), and the extent of the perturbations when propagating in a realistic model can be quantified by a norm difference between the propagation of a given set of initial conditions in both models. When comparing an error metric associated to the perturbed behavior to a user-defined threshold, the orbit may be classified as either "valid" when the metric is smaller than the threshold or "diverging" when it is larger. From a practical viewpoint, one must also consider the case of impacting trajectories which have a position magnitude that passes below the convergence radius of the spherical harmonic model at any point during the integration time span.

With this discrete measure of perturbation, the orbit data set behavior can be represented by plotting each orbit's behavior classification as a colored dot with coordinates given by intrinsic simplified model metrics, as shown in **Figure 11**. While the number of orbits of one classification can provide a single overall measure of the orbit set behavior against model perturbations, the plots shown indicate a likely relation of the orbit behavior in terms of pre-computed intrinsic AH3BP metric values used to represent the set. For example, the divergence appears to occur along particular families, and the family with periods between 200-300 hours does not appear to be unduly affected, while the periodic orbit families with periods between 300-450 hours exhibit mixed behavior. This separation is marked by the dashed black line in **Figure 11 (right)**.

Also emphasized on the plots are the regions with a notable lack of sample periodic orbits. This sparsity is due to the grid search technique used in generating the initial datase, where the number of intersections of an orbit with the x-z-plane was limited to 5 crossings. This constraint effectively bounds the range of periods (resonances) that can be captured in this representation. Regardless of this limitation, it appears that the range of orbits of a given classification (valid or diverging) is strongly dependent on the intrinsic characteristics of an individual orbit. The resulting problem is that of predicting perturbed orbit behavior as a function of these intrinsic AH3BP metrics. In a mission design setting, such a classification would enable a quick sorting

of valid orbits to be used in a given situation (and save the trouble of testing each orbit against one, or an ensemble of, representative models, as is performed in this study).

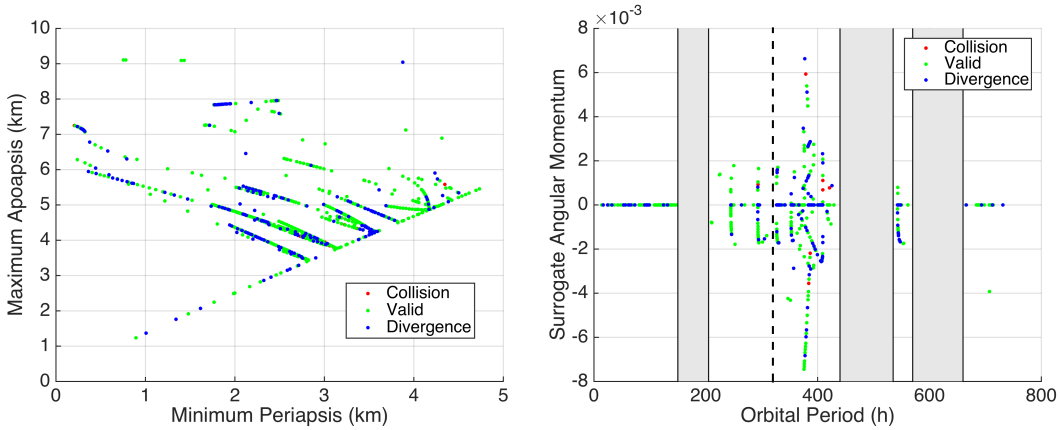

Figure 11. Sample orbit data set behavior represenation of the perturbed AH3BP ($\beta = 27$) with a divergence threshold of $\eta = 3$. Left: 2-D representation with apse distances as intrinsic orbit metrics. Right: 2-D representation with period and surrogate angular momentum as intrinsic orbit metrics with gaps in grid search results emphasized (grey regions).

These initial results depend to a large extent on the selected error metric threshold value to distinguish between valid and diverging behavior, as well as all of the other parameters used. It also assumes a transformation of the initial conditions from the AH3BP normalized state to the GER3BP physical units according to the constant length and time scales present in Hill's problem (referred to simply as Hill's scaling in the following). The results in **Figure 11** employed Hill's scaling, where the length and time scale are independent of the asteroid orbit. In the case of EV5, one normalized unit of length is equivalent to $\sim$47 km, while one normalized unit of time is $\sim$54.5 days. In the following sections, simpler cases are considered to further explore the influence of individual perturbations and the possible state transformations that can mitigate the number of observed diverging cases.

Effects of individual perturbations

As a first check on the influence of the asteroid orbit's eccentricity, the above plots were computed using both the fixed Hill's scaling and the elliptic AH3BP state transformation that has been discussed previously in the same set-up that was used for **Figure 11**. The Hill's scaling results indicate 47.5% of orbits remain classified as valid, while 51.8% remain in the elliptic scaling case, showing a small improvement due to the way in which the nominal normalized AH3BP initial conditions are transformed into the physical units of the GER3BP. Similarly, the number of impacting orbits decreases from 12.2% to 11.6% when the elliptic transformation is employed.

Similar experiments indicate that the number of diverging cases increases with the overall apoapsis radius, while the number of diverging orbits due to the increased complexity of the spherical harmonic model are localized to the vicinity of the small body. For example, **Figure 12** shows the comparison of the H3BP ($\beta = 0$) data set with a perturbed model that includes an 8×8 gravity field. As can be observed, most of the orbits with small apses radii become diverging with the presence of non-spherical gravitational perturbations (bottom left region of plots), while the distant orbits are much less affected. However, a few large orbits appear to be substantially affected by the introduction of these small forces.

Plotting the data as a function of the logarithm of the AH3BP maximum Lyapunov exponent (**Figure 13**) indicates that the orbits with the largest Lyapunov exponent within each family tend to diverge in the presence of this perturbation. This suggests a connection between the intrinsic linear stability of the periodic orbit and the medium fidelity behavior for non-spherical perturbations.

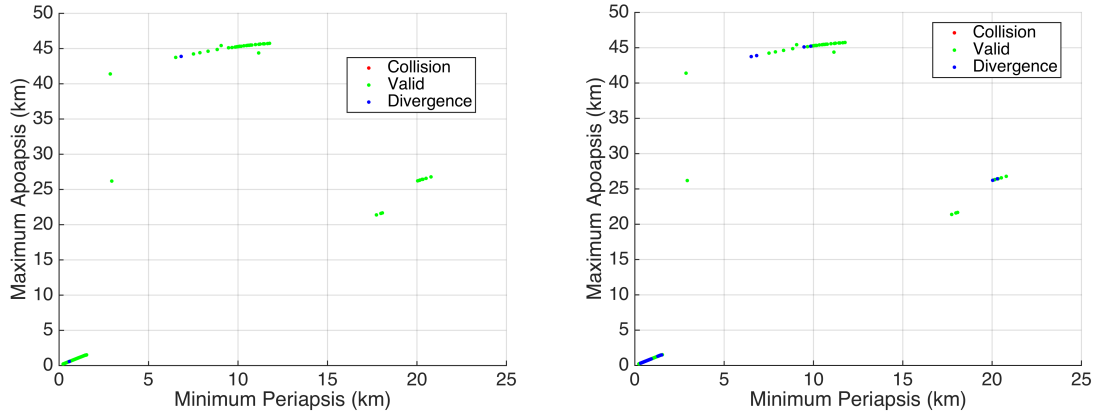

Figure 12. Orbit set behavior with a divergence threshold of $\eta = 0.05$ in the case of the Hill's problem ($\beta = 0$). Left: Point mass asteroid gravity. Right: 8×8 gravity field.

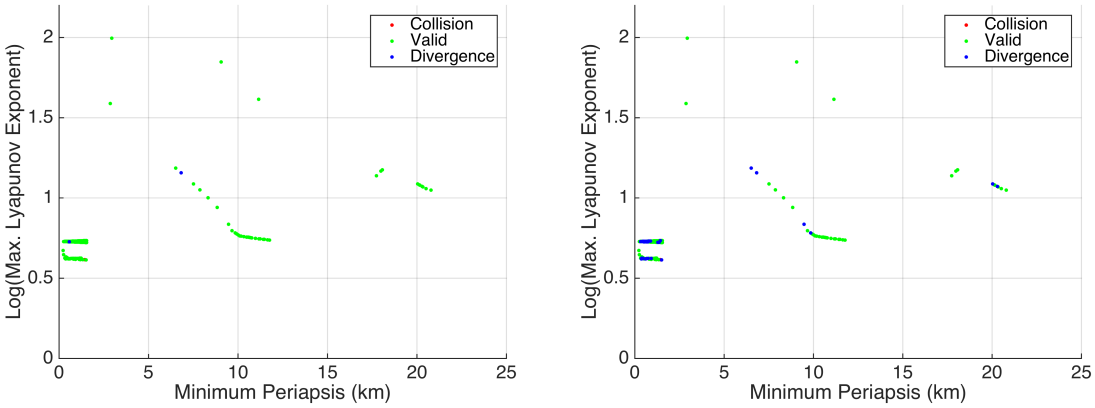

Figure 13. Orbit set behavior with a divergence threshold of $\eta = 0.05$ in the case of the Hill's problem ($\beta = 0$) as a function of minimum periapsis radius and logarithm of the maximum Lyapunov exponent. Left: Point mass asteroid gravity. Right: 8×8 gravity field.

Correlations with intrinsic metrics

As noted above, one goal of this study is the correlation of the intrinsic AH3BP metrics with the observed behavior in a perturbed model. While this relationship is still being investigated, **Figure 14** shows that the a priori expectation of a correlation of the divergence behavior with the maximum Lyapunov exponent and intrinsic sensitivity index is not quite as simple. In particular, there does not appear to be a specific maximum Lyapunov exponent value above which all orbits are classified as diverging (according to the current threshold of the error metric which defines divergence). Rather, the classification of the divergence behavior appears more closely related to the resonance properties of the orbits. The families which consist of orbits with very similar periods represent a given resonance relation in reference to other natural frequencies of the system (such as the asteroid orbital period) and clearly the destruction appears grouped in family rather than exponent level.

The natural frequencies of this system vary greatly in scale: the asteroid orbit has a period of $\sim$8200 hours, while the rotational period of the asteroid is $\sim$4 hours. Given the range of the periods of the main group of orbits considered (between 200 and 800 hours), the mean motion resonance relations are likely due to the

relations with the asteroid orbital motion, rather than its spin. For smaller orbits, this relationship is expected to be the opposite.

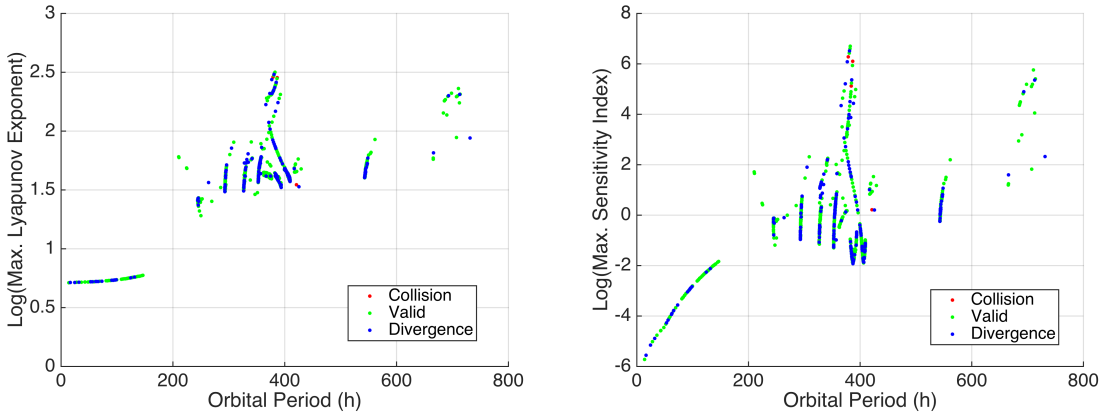

Figure 14. Representation of the orbit behavior of the AH3BP ($\beta = 27$) as a function of maximum Lyapunov exponent (left) and sensitivity index (right). The divergence threshold is $\eta = 3$ in this case.

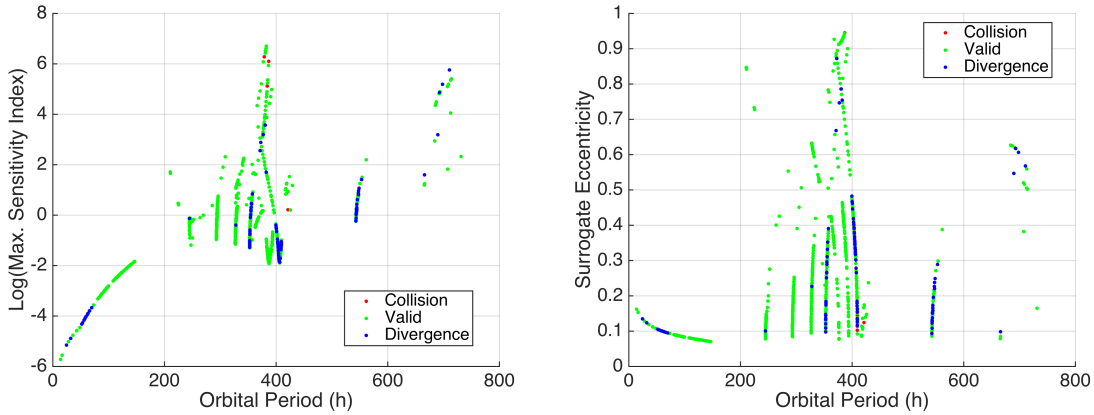

Figure 15. Representation of the orbit behavior of the AH3BP ($\beta = 27$) with elliptic scaling of the initial state prior to propagation. The divergence threshold is $\eta = 3$ in this case.

However, in both cases, the resonance relations are rather large (on the order of 1:10 and 100:1, respectively), and the coupling between spacecraft mean motion and its orbital precession of the line of apsides is likely the main dynamical mechanism in this set of data. Indeed, the visualization of a few trajectories (as shown in the previous sections), show that many of these families have apses organized symmetrically about the x-axis, forming petal shaped orbits (as in **Figure 7**). Nearby motion exhibits a slow rotational drift of this shape leading to other intrinsic frequencies associated with the orbit. The determination of the resonance relationship between these periods (mean motion and line of apsides) that would lead to more robust orbits would be of interest and needs further investigation.

This phenomenon is more keenly emphasized by the use of the elliptic Hill scaling of the initial state before propagation in the GER3BP. As shown in **Figure 15**, the reduction in the number of diverging cases for the same error measure threshold as was used for **Figure 14** shows that this state transformation improves the behavior and that the orbits appear to first diverge along particular families (resonances).

This situation is observed for a range of divergence threshold values, although both the Hill's and elliptic Hill's scaling techniques lead to mostly diverging cases if the error level is too tight. While the elliptic Hill's scaling approach is shown to generally result in more valid orbits, it does not account for the additional variation of the SRP perturbation throughout the course of the periodic orbit as the asteroid travels on its

elliptical heliocentric orbit. It is expected that applying an a priori transformation to the initial conditions to counteract this variation may also result in better behavior in the perturbed model.

CONCLUSIONS

This study explored the behavior of sample small-body periodic orbit databases (generated assuming the Augmented Hill's 3-body Problem dynamics) when transferred to realistic models. A numerical approach to the problem has been developed whereby orbital perturbations are measured by error metrics based on norm differences between orbits propagated in the simplified model and the perturbed model. These error metrics are used to categorize the behavior of each orbit in a set based on a user-defined threshold for divergence and this orbit behavior is then represented against intrinsic characteristics (such as the period, sensitivity index, and maximum Lyapunov exponent) of the orbits in the simplified model. This study emphasized error norms between trajectories, though similar norms on orbits (ignoring along track drifts) would also be relevant.

It was determined that the SRP is the dominant perturbation source in the observed behavior, causing many orbits to diverge, particularly as the asteroid moves on its orbit between perihelion and aphelion. The tendency of a periodic orbit to diverge when placed in a perturbed model appears to be related more to the resonance relationship (notably mean motion) of the spacecraft motion with the secular drift of the line of apsides for particular families of orbits, rather than a distinct threshold in the maximum Lyapunov exponents or sensitivity index.

It was also numerically shown that adjusting the transformation of the initial state from the simplified non-dimensional units to the physical units of the more complex model can mitigate to some extent the number of diverging orbits. In particular, the use of the pulsating length and time scales as derived from the elliptic Hill's three-body problem is shown to provide a small improvement over the fixed length Hill's scaling. However, it does not capture the effect of the varying SRP throughout the asteroid's orbit.

Further investigation of the dominant resonance relationships would be of interest to extend the use of simplified orbital models to a wide range of realistic asteroid setups. Statistical measures of orbit behavior classes, as well as cost of station keeping, should also be studied to provide a better characterization of the observed correlation between the intrinsic characteristics considered and the orbit behavior in perturbed models.

ACKNOWLEDGMENTS

This research has been sponsored by the AMMOS technology development task. A portion of the research presented in this paper has been carried out at the Jet Propulsion Laboratory, California Institute of Technology, under a contract with the National Aeronautics and Space Administration.

REFERENCES

[1] D. J. Scheeres, *Orbital Motion in Strongly Perturbed Environments: Applications to Asteroid, Comet and Planetary Satellite Orbiters*. Berlin, Germany: Springer-Praxis, 2012.

[2] D. M. Reeves, B. J. Naasz, C. A. Wright, and A. J. Pini, "Proximity Operations for the Robotic Boulder Capture Option for the Asteroid Redirect Mission," *AIAA SPACE 2014 Conference and Exposition*, No. AIAA 2014-4433, San Diego, California, August 4-7 2014.

[3] T. A. Pavlak, S. B. Broschart, and G. Lantoine, "Quantifying Mapping Orbit Performance in the Vicinity of Primitive Bodies," *25th AAS/AIAA Space Flight Mechanics Meeting*, No. AAS 15-389, Williamsburg, Virginia, January 11-15 2015.

[4] D. S. Lauretta and the OSIRIS-REx team, "An Overview of the OSIRIS-REx Asteroid Sample Return Mission," *43rd Lunar and Planetary Science Conference*, No. 2491, 2012.

[5] S. B. Broschart, G. Lantoine, and D. J. Grebow, "Quasi-Terminator Orbits Near Primitive Bodies," *Celestial Mechanics and Dynamical Astronomy*, Vol. 120, 2014, pp. 195–215.

[6] M. Giancotti, S. Campagnola, Y. Tsuda, and J. Kawaguchi, "Families of Periodic Orbits in Hill's Problem with Solar Radiation Pressure: Application to Hayabusa 2," *Celestial Mechanics and Dynamical Astronomy*, Vol. 120, July 2014, pp. 269–286.

[7] B. F. Villac, R. L. Anderson, and A. J. Pini, "Organizing Ballistic Orbit Classes Around Small Bodies," *AIAA/AAS Astrodynamics Specialist Conference*, No. AAS 15-619, Vail, Colorado, August 9-13 2015.

[8] E.Arnal Fort, B.Villac, J-M.Mondelo, "Exploration of a Graph Based Method for Orbital Transfers near Small Bodies," *2013 AAS/AIAA Astrodynamics Specialist Conference*, No. AAS 13-81, 2013.

[9] G. A. Tsirogiannis, "A graph based methodology for mission design," *Celestial Mechanics and Dynamical Astronomy*, Vol. 114, No. 4, 2012, pp. 353–363.

[10] D. J. Scheeres, "Stability of Hovering Orbits Around Small Bodies," *Advances in the Astronautical Sciences*, Vol. 102, No. 2, 1999, pp. 855–875.

[11] S. Sawai, D. Scheeres, and S. Broschart, "Control of Hovering Spacecraft Using Altimetry," *Journal of Guidance, Control, and Dynamics*, Vol. 25, July-August 2002, pp. 786–795.

[12] D. Scheeres, "Close Proximity Operations for Implementing Mitigation Strategies," *2004 Planetary Defense Conference: Protecting Earth from Asteroids*, No. AIAA-2004-1445, Orange County, CA, February 23-26 2004.

[13] S. B. Broschart and D. J. Scheeres, "Control of Hovering Spacecraft Near Small Bodies: Application to Asteroid 25143 Itokawa," *Journal of Guidance, Control, and Dynamics*, Vol. 28, March-April 2005, pp. 343–354.

[14] S. B. Broschart, *Close Proximity Spacecraft Maneuvers Near Irregularly Shaped Small-Bodies: Hovering, Translation, and Descent*. PhD thesis, The University of Michigan, 2006.

[15] S. B. Broschart and D. J. Scheeres, "Boundedness of Spacecraft Hovering Under Dead-Band Control in Time-Invariant Systems," *Journal of Guidance, Control, and Dynamics*, Vol. 30, March-April 2007, pp. 601–610.

[16] S. B. Broschart, G. Lantoine, and D. J. Grebow, "Characteristics of Quasi-Terminator Orbits Near Primitive Bodies," *Spaceflight Mechanics: Proceedings of the AAS/AIAA Spaceflight Mechanics Conference August held February 10-14, 2013 in Kauai, Hawaii* (S. Tanygin, R. S. Park, J. Thomas J. Starchville, and L. K. Newman, eds.), Vol. 148 of *Advances in the Astronautical Sciences*, San Diego, California, American Astronautical Society, Univelt Inc., 2013, pp. 953–968.

[17] G. Lantoine, S. B. Broschart, and D. J. Grebow, "Design of Quasi-Terminator Orbits Near Primitive Bodies," *AAS/AAIA Astrodynamics Specialist Conference*, No. AAS 13-815, Hilton Head Island, South Carolina, August 11-15 2013.

[18] D. M. Reeves, D. D. Mazanek, B. D. Cichy, S. B. Broschart, and K. D. DeWeese, "Asteroid Redirect Mission Proximity Operations for Reference Target Asteroid 2008 EV5," *39th Annual AAS Guidance and Control Conference*, No. AAS 16-105, Breckenridge, CO, February 5-10 2016.

[19] B.Villac and K.Y-Y.Liu, "Long-term Stable Orbits for Passive Tracking Beacon Missions to Asteroids," *Proceedings of the 2009 International Astronautical Congress (IAC)*, Vol. IAC-09.C1.10.6, 2009.

[20] S. B. Broschart and B. F. Villac, "Identification of Non-Chaotic Terminator Orbits Near 6489 Golevka," *AAS/AIAA Space Flight Mechanics Meeting*, No. AAS 09-156, Savannah, Georgia, February 9-12 2009.

[21] M. W. Busch, S. J. Ostro, L. A. M. Benner, M. Brozovic, J. D. Giorgini, J. S. Jao, D. J. Scheeres, C. Magri, M. C. Nolan, E. S. Howell, P. A. Taylor, J.-L. Margot, and W. Brisken, "Radar Observations and the Shape of Near-Earth Asteroid 2008 EV5," *Icarus*, Vol. 212, January 2011, pp. 649–660.